Wiley
International Journal of Distributed Sensor Networks
Volume 2024, Article ID 8644510, 18 pages
https://doi.org/10.1155/2024/8644510

Research Article

An Efficient Multisensor Hybrid Data Fusion Approach Based on Artificial Neural Networks and Particle Swarm Optimization Algorithms

Luc Eyembe Ihonock,[1] **Jean-François Dikoundou Essiben**,[1,2,3] **Benjamin Salomon Diboma**,[1,2,4] **and Joe Suk Yong**[5]

[1]*Technology and Applied Sciences Laboratory, University Institute of Technology of Douala, University of Douala, P.O. Box 8698, Douala, Cameroon*
[2]*Department of Electrical Engineering, Advanced Teachers' Training College for Technical Education (ATTCTE)-University of Douala, P.O. Box 1872, Douala, Cameroon*
[3]*Laboratory of Energy, Materials, Modeling and Methods, National Higher Polytechnic School of Douala, University of Douala, P.O. Box 2701, Douala, Cameroon*
[4]*Transport and Applied Logistic Laboratory, University Institute of Technology of Douala, University of Douala, P.O. Box 8698, Douala, Cameroon*
[5]*Department of Physics and Astronomy, Ball State University, Muncie, IN 47306, USA*

Correspondence should be addressed to Luc Eyembe Ihonock; eyembeluc@yahoo.fr

Received 24 May 2023; Revised 5 May 2024; Accepted 25 May 2024

Academic Editor: Ashish Bagwari

Copyright © 2024 Luc Eyembe Ihonock et al. This is an open access article distributed under the Creative Commons Attribution License, which permits unrestricted use, distribution, and reproduction in any medium, provided the original work is properly cited.

Data fusion plays a crucial part in performance evaluation processes in multisensor systems; thus, it is important to use an effective technique to cut down on errors. By improving the sensors' location and their capacity to adjust to the deployment geometry, the paper's technique for reducing data fusion errors is proposed. The preprocessing stage of data is also included in the suggested technique, which starts with the design of the data-collecting device and ends with a hybrid model algorithm. Particle swarm optimization and artificial neural network methods are combined in the hybrid algorithm. Preprocessing is based on the compensation and adjustment factors to ensure data gathering synergy. A true experimental apparatus was designed under three different deployment geometries, comprising five ultrasonic sensors constituting a multisensor system and a hardwood target (*Triplochiton scleroxylon* and *Milicia excelsa*). The results obtained show that the suggested deployment geometry has mean absolute percentage errors of 3.97, mean square errors of 0.182, and mean absolute errors of 0.045 which are lower than those associated with the deployment configurations found in the literature. The results of the proposed method show an overall detection accuracy in linear deployment geometry of 97.308%. Then, the circular deployment geometry obtained a detection accuracy of 97.005%. Finally, elliptical deployment geometry obtained a detection accuracy of 98.745%. These results show that the proposed method better predicts the range of a target with a lower error rate than conventional methods.

1. Introduction

The process of obstacle detection is challenging, complicated, and crucial since it requires taking into account a variety of targets, sensor properties, and ambient factors. Due to detecting constraints in terms of range, signal characteristics, and sensing circumstances, a single sensor can scarcely meet the demands of obstacle detection. As a result, researchers and engineers have developed a methodology for multisensor fusion and system integration [1]. When many sensors with the same or distinct technological qualities are combined to manage data, it is known as sensor data fusion [2]. One

essential element of system applications that employ linked data from several sources to ascertain a system's status is data fusion.

Data fusion should continue to be accurate and dependable when the system's condition is being monitored and the resources that are available change. It should also be able to adapt to the environment's changing dynamics and the available resources [3]. While determining a system's state, the data fusion must ensure fewer mistakes. Researchers are therefore interested in improving data fusion methods in multisensor systems. As a result, three methods (centralized, distributed, and hybrid) and algorithms for multisensor data fusion have been suggested [4]. The linear unbiased best estimate, weighted least squares, and their expanded forms are provided as optimum fusion rules and are implemented in a uniform architecture.

Using either identical sensors across the board or sensors of various types, centralized data fusion is a method that is employed [5]. The fusion method merges the unprocessed data from all sensors into a single processor. The data from all sensors must be time-synchronized for this operation. The amount of data gathered by the sensors is a factor in the choice made by this kind of fusion. Algorithms like the Kalman filter are coupled with the centralized data fusion method [6] and those that utilize probabilistic assumptions, like multi-Bernoulli [7]. The primary drawback of centralized data fusion is that it necessitates transferring all acquired data to a single processor, which is not practical for many applications.

Any sort of sensor, whether they are of the same type or distinct types, may be used in both centrally managed and decentralized data fusion systems. A Kalman filter can be used in conjunction with distributed data fusion [8] or techniques based on probabilities, such as the probabilistic data association filter [9]. The implementation of distributed data fusion uses a number of technologies, including GPS and SAR [10]. The central processor is freed from preprocessing the raw data from the various sensors in this design, increasing the percentage of uncertainty on the retrieved characteristics in the event of sensor failure.

The method for hybrid data fusion combines preprocessed and centralized fusion strategies. In actuality, several scholars believe that this architecture configuration is the finest [11]. This architecture is increasingly used in IoT [12], in mechanics for the indirect measurement of milling tool wear [13], combined with algorithms such as convolutional neural networks [14], Kalman filters [15], and probabilistic approaches [16]. The Kalman and Bayesian methods employed in hybrid data fusion are based on the Gaussian noise model; however, the noise may not always match this model. Also, the uncertainty produced while utilizing a neural network alone is not insignificant. Choosing the right number of hidden layers is usually a complex task. If this number is too small, it can lead to a poor estimate of the data generation process, while if it is too large, it can cause the problem of overadjustment and poor generalization of data [17]. This problem is accentuated if the data collected is of poor quality due to a lack of acquisition synergy in a multisensor system.

Problems with multisensor data fusion, such as data association and management, sensor uncertainty, data traffic, noise filtering, prediction making, and modeling dynamic systems, have drawn a lot of interest from the scientific community [18]. The uncertainties inherent in sensory information are not only caused by device inaccuracy but also by noise sources within the system and sensors [19]. As a result, increased focus is being made on using distributed multisensor data sources for a variety of applications, such as distributed system design and the use of scenario-based design techniques [20], monitoring, classifying, fusing information, and assessing the situation [21]. So, the key problem is to construct multisensor systems with an effective and straightforward method for minimizing mistakes.

The work motivation is based on the challenge of offering a technical solution to the designers of multisensor systems in order to increase performance. It is important that this solution be effective in reducing errors that arise from deployment geometries, data acquisition, and data fusion of multisensor systems. We will use the technique of artificial neural networks to solve the problem of optimal choice of learning rate and number of hidden layers by training this neural network with the PSO in order to offer a reliable and effective solution.

This research offers a more effective technique for fusing data from a sensor network, starting with the deployment geometry design, which depends on the false alarm probability and aperture angle, and finishing with an algorithm for preparing the data. When a target's range is estimated by a multisensor network, the PSO method and the neural network with a backpropagation algorithm are used to forecast and decrease error. These are the paper's primary contributions:

(i) the use of false alarm probability and aperture angle to design the elliptical deployment geometry to facilitate multisensor data fusion

(ii) the proposal of a multisensor data preprocessing algorithm based on the compensation coefficient in order to reduce the false alarm detection rate and to have a better data fusion synergy

Apart from the introduction, Section 2 gives a quick rundown of applications for hybrid data fusion and ultrasonic sensors. Section 3 presents a brief description of artificial neural network (ANN) and particle swarm optimization (PSO). The method is described in Section 4, with an emphasis on the algorithm of preprocessing, the ANN parameters that the PSO would optimize, and the experimental setup used to test the proposed method. In terms of the design and performance of the proposed method, the results and discussion are done in Section 5. This includes calculating the mean average percentage error (MAPE), mean square error (MSE), and mean average error (MAE). The findings and future work are presented in Section 6.

2. Related Work

2.1. Hybrid Data Fusion. Some classic data fusion techniques have flaws, which hybrid data fusion attempts to improve.

The classical approach used is to combine traditional data fusion methods with other efficient methods such as evolutionary algorithms (genetic algorithm and neural network) and metaheuristics (particle swarm optimization and ant colony optimization). Hybrid data fusion technology is an important data processing method that has a wide range of applications, such as target detection [22], medical diagnosis [23], remote sensing mapping [24], and object recognition [25]. Traditional data fusion methods that are used to build hybrid data fusion methods are mainly divided into three groups: (1) methods based on probability, (2) Dempster-Shafer theory, and (3) knowledge methods [26]. Methods based on probability for data fusion are focused on the dependence between random variables by introducing the probability distribution and probability density function. These methods include Bayesian inference [16], the Kalman filter model [15], and the Markov model [27].

A robust incremental Kalman filtering algorithm has been proposed and introduced in the incremental formula to remove unknown measurement errors from the data acquisition system [28]. The transition probability and noise matrix of the system are adjusted using an adaptive multimodel-extended Kalman filter estimation approach based on velocity and flow to decrease estimation error [29]. A weighted fusion method for real-time outlier separation and correction is developed to solve the problem of the decreasing accuracy of data processing [30]. A weighted hierarchical multisensor fusion algorithm for maneuver target tracking obtains its model by hierarchical weighting and estimates the state using an extended Kalman filter [31].

The fusion data method, based on Dempster-Shafer (D-S) theory, expresses data uncertainty by introducing confidence and rationality in dynamic situations. A weighted combination method for conflicting evidence in multisensor data fusion by considering both the interaction between the impacts and the evidence themselves (sensors) was developed in [32]. Target recognition with a sensor network is also possible with a multilocation parallel fusion method based on D-S evidence theory [33]. A multisensor information fusion failure diagnosis method based on the sample entropy for empirical mode decomposition and improved D-S evidence theory was proposed [34]. Dempster-Shafer and adaptive neuro-fuzzy inference are used for hybrid fusion of information data with restricted content [35].

The knowledge-based fusion method mainly uses support vector machine (SVM) and clustering to find the knowledge contained in the data and to measure the correlation and similarity of the knowledge. A hybrid multisensor data fusion algorithm based on fuzzy clustering is proposed as a strategy to determine the initial clustering center [36].

Deep learning is a popular algorithm in general engineering, and a review of the state of the art is done to understand deep learning and draw the benefits to optimize data fusion [37]. To improve wireless sensor network data fusion, a data fusion algorithm based on a gray wolf algorithm and a backpropagation neural network was proposed [38]. The bidirectional multiresidual recurrent neural network, integrating past and future information at each time with an omniscient attention model, is proposed in [39]. In order to identify the best weights, a new data fusion technique that employs a global Kalman filter and a measurement variance prediction long-term memory network is provided [40]. An intelligent data fusion system for damage detection was suggested using a probabilistic neural network, data fusion technology, and correlation fractal dimension [41]. Waveform-based fault diagnosis is an increasingly used technique [42], and a convolutional neural network is used to increase the detectability of faults [43]. Intelligent diagnosis approaches based on neural networks tackle the data count problem, which improves the performance of neural network techniques. Some make use of neural networks and adversarial learning methods [44]. Some employ an approach known as the threshold criteria to assess when an unknown source error occurs during real-world diagnostics [45]. Deep learning based on stacked sparse autoencoders and multisensor fusion is used to predict milling tool wear prediction [46]. For the works that have used artificial neural networks, very few have focused on the optimization of parameters such as the learning rate and the number of hidden layers of the artificial neural network, which are nevertheless very decisive for its performance.

2.2. Hybridization of Neural Networks with PSO. Neural networks (RNs) have progressed as valuable machine learning techniques that are extensively employed in a variety of studies. At the moment, RN is a sophisticated method for extracting information from enormous datasets in a self-organized manner [47]. Deep neural networks (DNNs), for example, contain various architectures and parameters that are usually tailored to specific applications. Furthermore, defining the most exact and practical structure of a deep learning approach within an acceptable time frame may prove problematic [48]. The classic backpropagation (BP) technique has been superseded by particle swarm optimization (PSO) as a potential choice for ANN training. The PSO offers benefits owing to its extensive research capability, fast convergence, and ability to provide the best overall solution [17]. Metaheuristic techniques have been widely investigated in the development of feedforward neural network (FFNN) to control the shortcomings of gradient-based and backpropagation algorithms with peculiarities [49]. Even though the PSO provides a solution for selecting the design parameters of many types of neural networks, this performance can only be achieved with a large quantity of data. However, inaccurate data gathering by a multisensor system might lead to poor neural network parameter creation. The hybridization of PSO and FFNN shows the need to use a preprocessing algorithm, which would boost hybridization efficiency and create data collection synergy.

2.3. Ultrasonic Sensors. The improvement can be done in different ways, including data collection and transmission, sensor fusion, data analysis, security, and privacy [50]. With the evolution of electronic devices, nowadays, there is a panoply of sensors allowing us to conduct measurements aiming to better understand phenomena [51]. In the automotive field, several works have been carried out to detect and avoid obstacles by increasing the efficiency of driving

by implementing various control strategies [52]. The instrument used for distance measurement in obstacle avoidance is ultrasonic sensor(s) combined with algorithms such as deep learning [53]. A multisensor ultrasound system is used to assess the road traffic of pedestrians, cyclists, and slow-moving vehicles to improve driver assistance systems [54]. The ultrasonic sensors are mainly used in automatic parking assistance systems for vehicles in the parking lot [55]. The performance of ultrasonic sensors in detecting different obstacles is improved by using fuzzy logic [56]. In automated guided vehicles, a multisensor ultrasonic system combined with Kalman filtering is used to improve navigation performance [57]. Dynamic tracking of surrounding objects in traffic environments using Kalman filtering algorithms can be improved with a cost-effective ultrasonic sensor network [58]. The evaluation of the efficiency of ultrasonic sensors against certain failures and their mathematical models is a subject of concern to researchers [59, 60]. To reduce errors in the distance measurement performed by the ultrasonic multisensor system by using Newton's polynomial [25, 61], artificial neural network [62], and fuzzy logic [63], distance measurement in an indoor environment is confronted with several error-increasing phenomena. In order to reduce errors, a multisensor system is combined with a Kalman filter [64, 65].

In civil engineering, ultrasonic sensors can be used to optimize the maintenance service in buildings [66], for the design of intelligent lawn mowers [67]. The 2-D mapping of a building uses ultrasound sensors to reduce the problem of specular reflections [68]. In the field of medicine, ultrasound sensors are used to detect falls in the elderly using a support vector machine and long-term memory as a classifier [69, 70]. Many ultrasound sensor devices are designed to help the blind move around, and some use collision avoidance methods for navigation aids [71]. Other researchers are developing digital solutions to enable blind people to travel [72].

A smart cane-based state-feedback control technique has been presented for a multisensor obstacle detection system to manage the sensors' detecting angles and reduce false warnings to the blind [73]. Researchers are working to create a prototype ultrasonic sensor-based smart cap as an electronic travel assistance for blind individuals [74]. The arrival of the coronavirus prompted engineers to design a distancing device using social engineering through an awareness network to slow the spread of the virus [75].

In addition to their traditional applications, ultrasonic sensors may be used to investigate the aquatic environment [76]. Ultrasonic sensors are also used in municipal solid waste collection to measure the level of waste in order to optimize collection rounds [77]. Ultrasonic sensors are increasingly used in agriculture to study plant growth for characterization [78]. The ultrasound sensor is also used as a radar [79]. Ultrasonic sensors are used to evaluate the load measurement efficiency of high furnaces [80]. This is also the case for mapping indoor environments in virtual reality without light [81]. Other uses of ultrasonic sensors include localization and navigation in indoor environments using a circular network [82]. The fusion technology of wide-angle ultrasonic sensor and inclination sensor is applied nowadays to the attitude monitoring of advanced hydraulic support [83]. In order to decrease measurement error as much as feasible given the growing usage of ultrasonic sensors in all real-world and everyday applications, it is critical to look beyond the so-called traditional research fields and suggest new ones.

3. Brief Description of Artificial Neural Networks and Particle Swarm Optimization

3.1. Artificial Neural Networks. Effectively adjusting to the signal randomness, neural network-based approaches produced fewer prediction mistakes [84]. Among the different artificial neural networks (ANNs), there is the feedforward artificial neural network (FANN) with p input nodes, h hidden nodes, and a single output node:

$$y_t = G\left(\alpha_0 + \sum_{j=1}^{h} \alpha_j . F\left(\beta_{0j} + \sum_{i=1}^{p} \beta_{ij} y_{t-i}\right)\right), \quad (1)$$

where α_j and $\beta_{ij} (i = 1, 2, \cdots, p\,; j = 1, 2, \cdots, h)$ are the connection weights, α_0 and β_{0j} are the bias terms, and F and G are the network activation functions. There are also several input and output networks, as shown in Figure 1. The selection of the appropriate network structure is crucial to the success of the ANN model, despite its simplicity and immense popularity in several fields such as wind energy forecasting [85] and the optimal placement of photovoltaic systems [86].

The selection of an appropriate number of hidden nodes is in general a complicated task [87]. To solve the problem of the number of hidden layers, one uses the Bayesian information criterion (BIC) to determine the appropriate network architecture.

$$\mathrm{BIC} = N_{p,h}(1 + \ln\,(n)) + n \ln\left(\frac{S(W)}{n}\right), \quad (2)$$

where $N_{p,h} = h(p + 2) + 1$ is the total number of network parameters; $n = N_{\mathrm{train}} - p$ is the number of actual observations, where N_{train} is the size of the training set; $S(W)$ is the misfit function representing the sum of the squared errors (SSE) between the actual and predicted observations; and W is the space of all connections of all weights and biases. The best network structure is determined by minimizing the BIC value.

The optimal weights and biases are determined iteratively with the objective of minimizing the function SSE. The backpropagation (BP) algorithm successively updates the weights and biases of the network to minimize the SSE [88].

$$E(W) = \frac{1}{2} \sum_{t=p+1}^{N_{\mathrm{train}}} (y_t - \widehat{y}_t)^2, \quad (3)$$

where y_t and $\widehat{y}_t$ are the actual and target values, respectively. The BP algorithm starts with an initial vector W_0 of weights

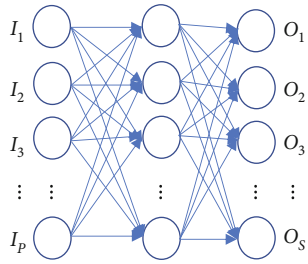


Figure 1: Feedforward neural network.

and biases and then updates it iteratively at each i-step by the gradient descent rule.

$$\left.\begin{aligned} \Delta W_i &= -\eta \nabla E(W)\big|_{W=W_i} + \alpha \Delta W_{i-1} \\ W_i &= W_i + \Delta W_{i-1} \end{aligned}\right\}, \tag{4}$$

where α and η are the learning rate and the momentum factor, respectively. The learning stops when a predefined value of the minimum error is reached.

Despite its simplicity and immense popularity, the BP algorithm has a number of limitations, including a long computation time, a slow convergence rate, a complex error surface model, and bogging down in local minima [88].

3.2. Particle Swarm Optimization. The particle swarm optimization (PSO) method uses social interaction among independent particles to determine the least and maximum value of a function. The PSO algorithm has two parameters, location and velocity, which are updated for each particle and in all dimensions considered. PSO demonstrates its distinctive qualities, including ease of implementation, consistency in performance, and the capacity to quickly converge on many complicated optimization problems [89]. In this approach, the entire population is considered a single neighborhood for that particle during the experiment acquisition process. In this algorithm, the velocity of the i^{th} particle, v_i^{k+1} is updated.

$$v_i^{k+1} = \theta v_i^k + c_1\beta_1\left(p\varphi_i - x_i^k\right) + c_2\beta_2\left(g\varphi_i - x_i^k\right), \tag{5}$$

where β_1 and β_2 are two random numbers between zero and one; x^k and v^k are the position and velocity of the i^{th} particle in the k^{th} iteration, respectively; $g\varphi_i$ is the best position experienced by the set of particles; and $p\varphi_i$ represents the best personal experience of the particle. θ is called the inertia constant. c_1 and c_2 are constants called the personal learning factor and social learning factor, respectively. The update of the particle's position is done according to equation (6), which follows:

$$x_i^{k+1} = x_i^k + v_i^k, \tag{6}$$

where x_i^{k+1} is the new position of the particle, x_i^k is the previous position of the particle, and v_i^k is the new velocity obtained from equation (5).

To control the dynamic characteristics of the particle swarms and the balance between the local and global search, a factor limiting is applied.

$$\theta = \frac{2\beta}{\phi - 2 + \sqrt{\phi^2 + 4\phi}}, \tag{7}$$

where $\phi = \phi_1 + \phi_1 > 4$.

$$\left.\begin{aligned} c_1 &= \phi_1\theta, \\ c_2 &= \phi_2\theta, \end{aligned}\right\}, \tag{8}$$

where ϕ_1 and ϕ_1 are positive random numbers from a unified distribution, where ϕ is their sum, must be greater than 4, and β is a value between zero and one. Moreover, θ is known as the restriction factor. Each particle evaluates its own fitness function (usually of type SSE).

4. Method

4.1. Proposed Approach of Multisensor Data Fusion. This work is aimed at reducing the method of implementation of the multisensor system and the environment, which affects the signal strength received by the sensors. The proposed approach consists of four steps:

Step 1. Design of the data acquisition system.

The elliptical deployment shape is designed in this part to enhance the quality of the data gathered because the deployment geometry is a key idea in data fusion for multisensor systems. A significant factor in the quality of the data is the distance between the sensors. When applied to targets with complicated geometries, linear and circular geometry are frequently ineffective. A 2-D parametric equation (9) describes the proposed geometric configuration.

$$x = x_0 + a\cos(t), \tag{9}$$

$$y = y_0 + b\sin(t), \tag{10}$$

where x_0 and y_0 are the coordinates of the center of the ellipse; a and b are parameters for the length on the x-axis and y-axis, respectively; and t is the aperture of the ellipse. The proposed approach consists of determining a and b while respecting the principles of spotlight formation in synthetic aperture radar systems, as shown in Figure 2.

Let us consider a multisensor system formed of N sensors aligned, as illustrated in Figure 3, where Ω is the aperture angle. The deployment geometry is symmetric with an odd number of sensors. By considering the triangles (OEB) and (OAB), we can express $\cos(\Omega/2)$ according to the equations (11) and (12), $\cos(\Omega/2) = OB/OE$ and $\cos(\Omega/2) = OA/OB$, respectively.

By multiplying the two values, we obtain

$$\cos^2\left(\frac{\Omega}{2}\right) = \frac{OA}{OE}, \tag{11}$$

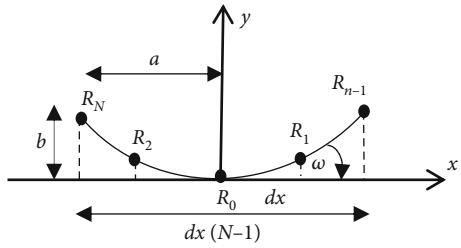


Figure 2: Elliptical sensor deployment.

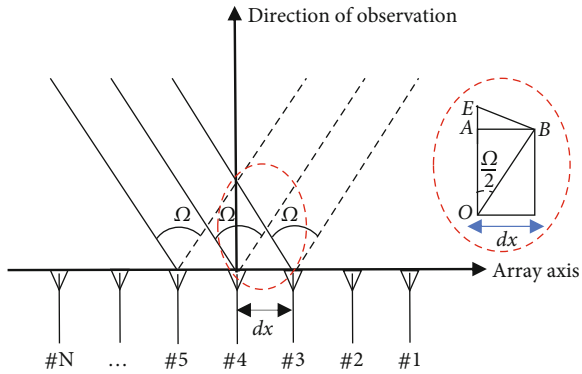


Figure 3: Geometry of calculation of spacing.

where $OA = OE \times \cos^2(\Omega/2)$, $OE = \xi \times D$, with ξ, which is the proportion of the main lobe power corresponding to the beam width from one null to another in the wave propagation plane. The choice of the value of ξ is made according to the probability of false alarm. Let us consider the triangle (OAB), we have $dx = OA \tan(\Omega/2)$ with $AB = dx$. The regular spacing between the sensors is calculated using the following equation:

$$dx = \xi D \cos\left(\frac{\Omega}{2}\right) \sin\left(\frac{\Omega}{2}\right). \tag{12}$$

The aperture length, or so-called deployment length, which is a function of N and the sensor spacing dx, is where the parameter a is obtained from.

$$a = \frac{dx\,(N-1)}{2}. \tag{13}$$

The parameter value b is a compromise between the tilt angle and the deployment length a.

$$b = \frac{dx(N-1)\tan(\omega)}{2}. \tag{14}$$

Replacing dx by its expression, we obtain the following equation:

$$b = \frac{\xi D \cos(\Omega/2) \sin(\Omega/2)(N-1)\tan(\omega)}{2}. \tag{15}$$

Step 2. Data preprocessing and storage.

The use of an adjustment factor is suggested to help in the distance estimates between the sensor and the target when the signal-to-noise ratio fluctuates for the same distance. This factor δ is the ratio between the actual distance d_a and the average measured distance d_m after a measurement time to have a good calibration in the deployment environment of the sensor.

$$\delta = \frac{d_a}{d_m}. \tag{16}$$

The estimated distance d_s for each sensor can be expressed according to the following equation:

$$d_s = \delta d_i, \tag{17}$$

where d_i is the instantaneous distance measured at a time t. Hence, the average distance expressed by the system of N sensors is

$$D_{s_m} = \frac{1}{N} \sum_{n=0}^{N-1} \delta_n d_{s_n}. \tag{18}$$

Data fusion may be challenging for multisensor systems since the final data quality would suffer if one sensor transmits an erroneous measurement result. It is suggested that the deployment system be symmetric and that the sensor at the center of symmetry be used as the reference sensor in order to improve the data acquisition process. The symmetry configuration will maintain that the main lobe is always perpendicular to the target. To keep the consistency and synergy of the measurements between the sensors, the compensation factor k is used. The compensation factor k is the ratio between the distance d_{s_n} estimated by a sensor and the distance d_{s_0} estimated by the reference sensor:

$$k_n = \frac{d_{s_n}}{d_{s_0}}, \tag{19}$$

where $n = 0, \cdots, N-1$. For the system to validate the value of d_s given by a sensor, the value of the compensation factor (k_n) linking the sensor to the reference sensor must be respected. The value of the compensation factor is used to reduce the occurrence of false measurement values.

Step 3. Search for optimal parameters of the backpropagation neural network using PSO.

The role of the PSO is to optimize the number of hidden layers and the learning rate between layers of the neural network. The approach used to optimize the number of hidden layers and the learning rate is described as follows: the neural network structure has structures $p \times h \times 1$ and N_{swarm}, and the swarm size and each particle represent an individual

ANN of dimension $\Gamma = h(p+2)+1$, which is the total number of network parameters.

Equations (5) and (6) permit the PSO algorithm to update the particle's velocity as follows:

$$v_{id}^{k+1} = \theta v_{id}^{k} + c_1\beta_1\left(p\varphi_{id} - x_{id}^{k}\right) + c_2\beta_2\left(g\varphi_{id} - x_{id}^{k}\right),$$
$$x_{id}^{k+1} = x_{id}^{k} + v_{id}^{k}, \tag{20}$$

where $i = 1, 2, \cdots, N_{\text{swarm}}$; $d = 1, 2, \cdots, D$; v_{id}^{k+1}; and x_{id}^{k+1} are, respectively, the velocity and position of the i^{th} particle in the d^{th} dimension and $p\varphi_{id}$ and $g\varphi_{id}$ are, respectively, the best personal and global positions obtained so far in the d^{th} dimension. The position of each particle is calculated by a particular fitness function SSE. The PSO algorithm keeps updating locations and velocities up until the stopping requirement, such as the maximum number of iterations, is met. When the number of input layers is known when employing the backpropagation algorithm, when the halting condition is reached, we have an SSE corresponding to one dimension, which lets us know the number of hidden layers and the learning rate.

Step 4. Training and using the backpropagation neural network with optimal parameters.

The PSO scans the search space to get the ideal hidden layer and learning rate settings that minimize the neural network's prediction error. At each value of the parameters obtained by the PSO, the neural network is trained up to the PSO stopping criterion. The PSO will scan the whole search space and choose the neural network with the best SSE value in terms of minimization to create the network with the ideal parameter values. Then, the trained, optimized neural network is used to estimate the range of the target. Figure 4 displays the flowchart that summarizes the processes in Step 2 and Step 3.

4.2. Experimental Setup. The simplified schematic in Figure 5 depicts the experimental acquisition data set-up. The experimental device consists of four parts, including a target, five identical ultrasonic sensors, an acquisition board, and a computer. The target is fashioned of *Milicia excelsa* and *Triplochiton scleroxylon*, two common tropical woods in Cameroon, and measures 1.6 meters in height and 0.55 meters in breadth. The front face is made of *Triplochiton scleroxylon* (ayous), and the front sides are made of *Milicia excelsa* (iroko). The ultrasonic sensors (HC-SR04) have an accuracy of 3 mm over a range of 5 m with an opening angle of 15°. The data acquisition board is an Arduino UNO-type board, and its role is to extract the distance feature from the signal coming from the sensors. The PC has a Core i5, 4GB of RAM, and MATLAB 2020 software is employed. The multisensor system's calculated distance average is stored by the system in a database. This data will be used as input for the method. The data collection serving as input for our method is done in 50 minutes, producing 3000 points of data on a total measurement distance of 5 m.

5. Results and Discussions

The raw data of this study are the mean values of several tests (three for each step), where the standard deviation between the different tests for all tested steps is between 0.724 and 1.327. The flowchart in Figure 6 describes the proposed algorithm to improve the performance. The data used for training and validation are from our previous work [90]. The percentage of 80% of the data used is considered training data, 10% is used for validation, and 10% is considered test data for the neural network. The number of neurons in the output layer is 50, and due to the crucial role of the number of neurons in the hidden layer, its number is considered according to Levenberg-Marquardt. In the case of the ultrasonic sensor (HC-SR04) and in our test environment, this adjustment coefficient is $\delta = 0.980$. The spacing dx between the different sensors with the opening angle of the reference sensor equal to 15° and $\eta = 0.082$ is 5 cm. It is therefore important to determine the spacing between the different sensors since bad spacing can increase losses due to the modulation of the main lobe. Table 1 shows the values of each parameter used to design each deployment geometry: a_R and a_I are each the elliptical parameters for regular and irregular spacing, respectively, and R_R and R_I are each the radius of the circle for regular and irregular spacing, respectively.

The proposed method is to determine the optimal value of the number of hidden layers and the learning rate using the PSO so that the ANN is more efficient in data fusion. The stopping criterion of the PSO is the number of iterations, and its parameters are summarized in Table 2.

Tables 3 and 4 show the influence of the number of particles in the PSO algorithm on the optimal determination of the number of hidden layers and the learning rate of the neural network. In Tables 3 and 4, we make a comparative study. The parameters of this study are the correlation coefficient given by the neural network, the optimal value of the learning rate, the number of hidden layers, the type of spacing between the sensors, and the population size of the particle swarm. The analysis of Tables 3 and 4 shows us that the number of PSO particles is a crucial parameter for the training of the neural network by the PSO [51].

The value of the learning rate is also a function of the input data and, therefore, of the deployment geometry of the data acquisition device, as shown in Tables 3 and 4. The value of the learning rate α is constant in Table 3 at $N_{\text{swarm}} = 20$ in regular spacing, while in Table 3, in irregular spacing, α is constant at N_{swarm} equal to 14 and 20. The value of the number of hidden layers decreases when the value of the number of PSO particles increases, which corresponds to the analysis in [51]. In Table 3, the elliptical geometry has better correlation coefficients than the geometries linear and circular used in this work. At $N_{\text{swarm}} = 20$, in regular spacing (Table 3), the linear geometry has 0.054%, and the elliptical geometry has 0.058% better correlation coefficients than [56, 75]. In irregular spacing (Table 4), the linear geometry is 0.059%, and the circular geometry is 0.1% better than [51, 75] for the correlation coefficient parameter. In the following, all the results presented are for $N_{\text{swarm}} = 20$.

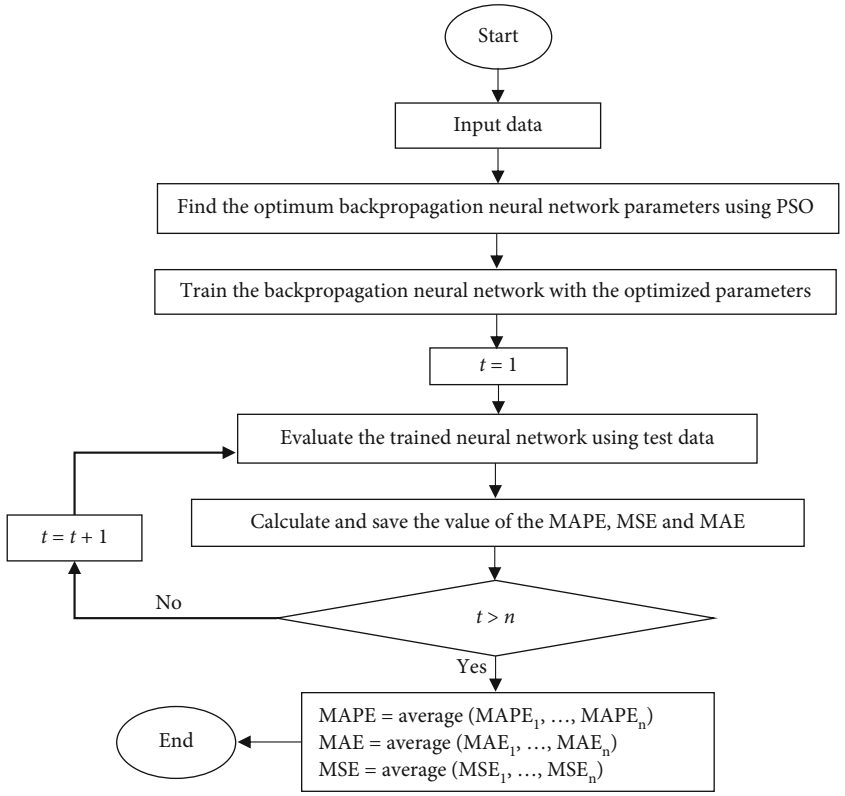


Figure 4: The flowchart of the proposed method.

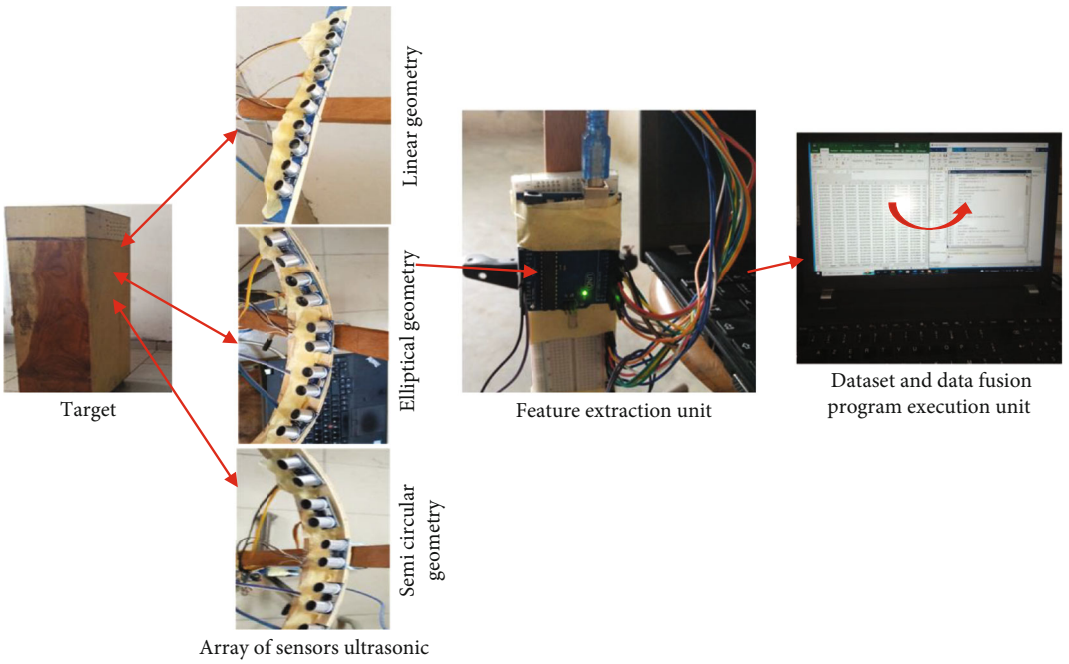


Figure 5: Simplified diagram of the experimental setup.

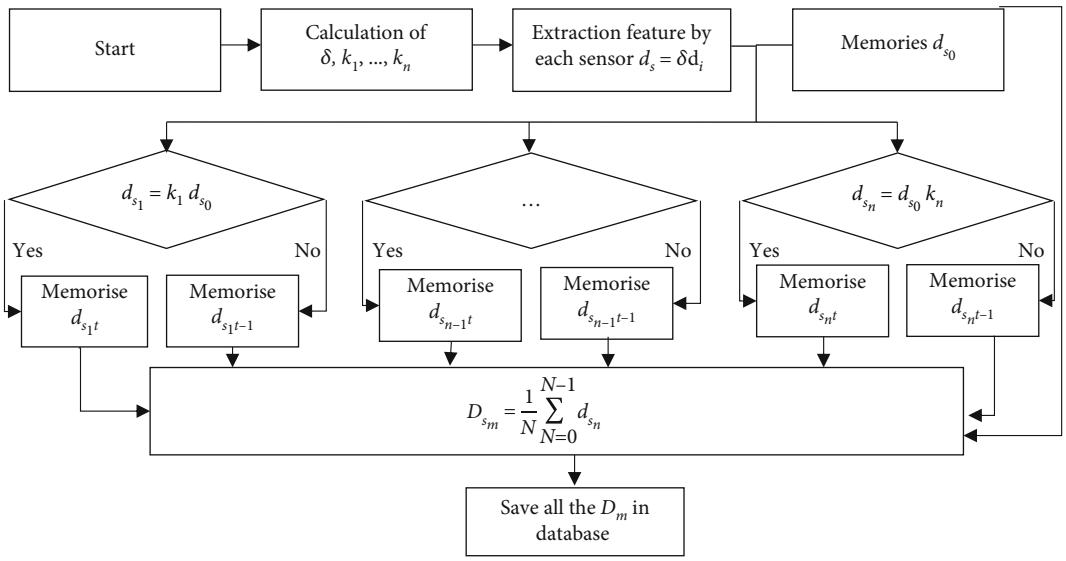


Figure 6: Flowchart of the data fusion process.

Table 1: Parameter design of the geometry deployment.

Geometry deployment	Regular spacing	Irregular spacing	Design parameters	Rayon of circle	N
Linear	5 cm	7 cm and 13 cm	/	/	5
Circular	5 cm	7 cm and 13 cm	/	$R_R = 10$ cm; $R_I = 13$ cm	5
Elliptical	5 cm	7 cm and 13 cm	$a_R = 10$; $a_I = 13$ cm; $b = 5.679$ cm	/	5

Table 2: PSO parameters.

Number of iterations	1500
Acceleration factors	$c_1 = 1.332$ and $c_2 = 2.339$
Sum of random numbers from a unified distribution (ϕ)	4.8
Restriction factor (θ)	0.7529

Table 3: Variation of neural network parameters when sensors are in regular spacing.

N_{swarm}		10			15			20	
Deployment geometries	h	α	R	h	α	R	h	α	R
Linear	70	0.481	0.945	20	0.377	0.997	15	0.307	0.999
Circular	70	0.181	0.992	20	0.407	0.993	15	0.307	0.996
Elliptical	70	0.369	0.997	20	0.377	0.998	15	0.307	0.999

Table 4: Variation of neural network parameters when sensors are in irregular spacing.

N_{swarm}		10			15			20	
Deployment geometries	h	α	R	h	α	R	h	α	R
Linear	70	0.125	0.977	20	0.377	0.998	15	0.307	0.999
Circular	70	0.328	0.997	20	0.377	0.999	15	0.307	1
Elliptical	70	0.394	0.999	20	0.377	0.999	15	0.307	0.997

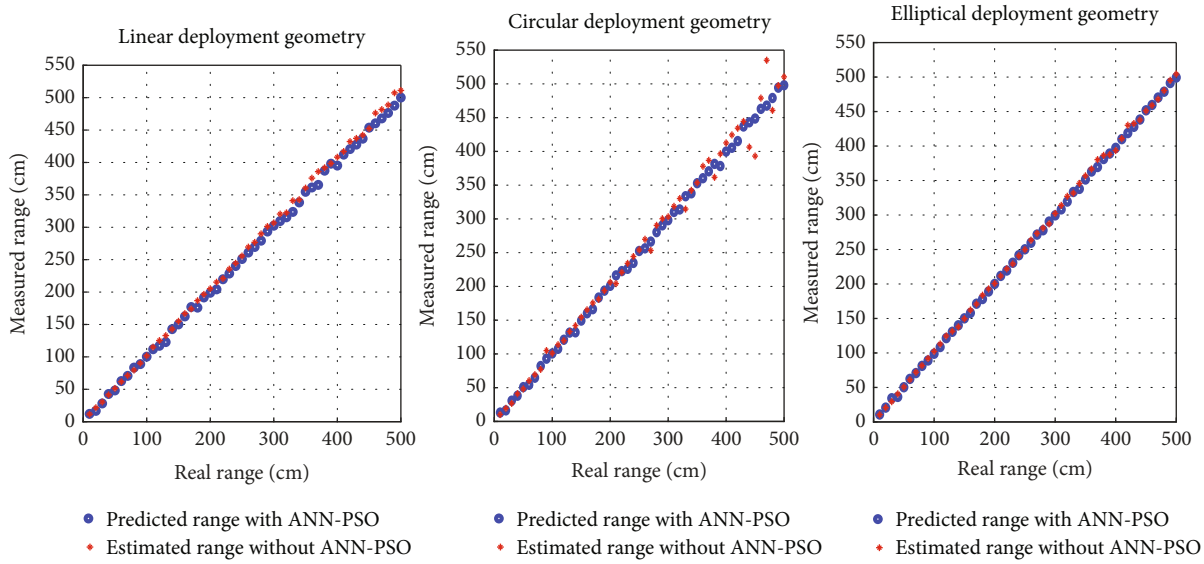


Figure 7: Estimation of the target-device range under three deployment geometries with regular sensor spacing.

Table 5: Comparison of errors as a function of regular spacing deployment geometries.

Real range (cm)	[79]		Proposed method					
			Linear deployment geometry		Circular deployment geometry		Elliptical deployment geometry	
	Estimated range (cm)	Error (%)	Predicted range by the proposed method (cm)	Error (%)	Predicted range by the proposed method (cm)	Error (%)	Predicted range by the proposed method (cm)	Error (%)
40	39.64	0.9	42.74	6.85	38.11	4.725	36.31	9.225
80	78.98	1.275	83.45	4.3125	82.07	2.587	81.28	1.6
120	120.92	0.76	117.1	2.41	121	0.83	121.5	1.25
160	161.4141	0.88	162.4	1.5	160.2	0.125	158	1.25
200	200.3333	0.16	198.9	0.55	200.9	0.45	200.1	0.05
240	208.1414	13.27	240.2	0.083	234.8	2.16	241.7	0.70
280	206.7475	26.16	279.3	0.25	280.4	0.14	277.9	0.75
320	206.46	35.43	315.4	1.437	314.6	1.68	319.5	0.15
360	206.62	42.60	361.4	0.38	360.3	0.083	363.1	0.861
400	206.79	48.30	395.2	1.2	399.8	0.05	397.4	0.65

It is worth noting that the number of iterations and particles has a significant impact on the execution time of the proposed hybrid algorithm. In this situation, the greater the number of particles, the longer the execution time; hence, it is critical during hybridization to strike a balance between the number of iterations, particles, and execution time for real-time applications.

Figure 7 shows the target-device range data with regular spacing between the sensors under three deployment geometries on actual values. The data predicted by the proposed fusion method (ANN-PSO) are in blue and the noisy data are in red. A comparison of the results between those predicted by the proposed fusion method and those estimated by the data acquisition device is made. A significant improvement in the performance of the multisensor system could be achieved with the algorithm by applying the proposed data fusion method. The analysis in Figure 7 shows that in both linear and elliptical geometry, along the maximum test range, the measurements follow a quasilinear form. This evolution shows that the signal-to-noise ratio is almost linear. This contact remains true in circular geometry in the interval [0; 400] cm, which is not the case in the interval [410; 500] cm. The measurements obtained on the maximum test range have a maximum error value of 47 cm, representing an increase of more than 7% in circular geometry, 11.11 cm or 2.222% in linear deployment geometry, and 4.34 cm or 0.868% in elliptical deployment geometry. Note that the elliptical geometry has better range estimation accuracy than the circular and linear geometry when the spacing between sensors is regular.

Table 5 shows a comparison of an extract of the values between the range values estimated by the proposed data fusion method and by the device (raw) when the sensors are in regular spacing and those taken from the literature.

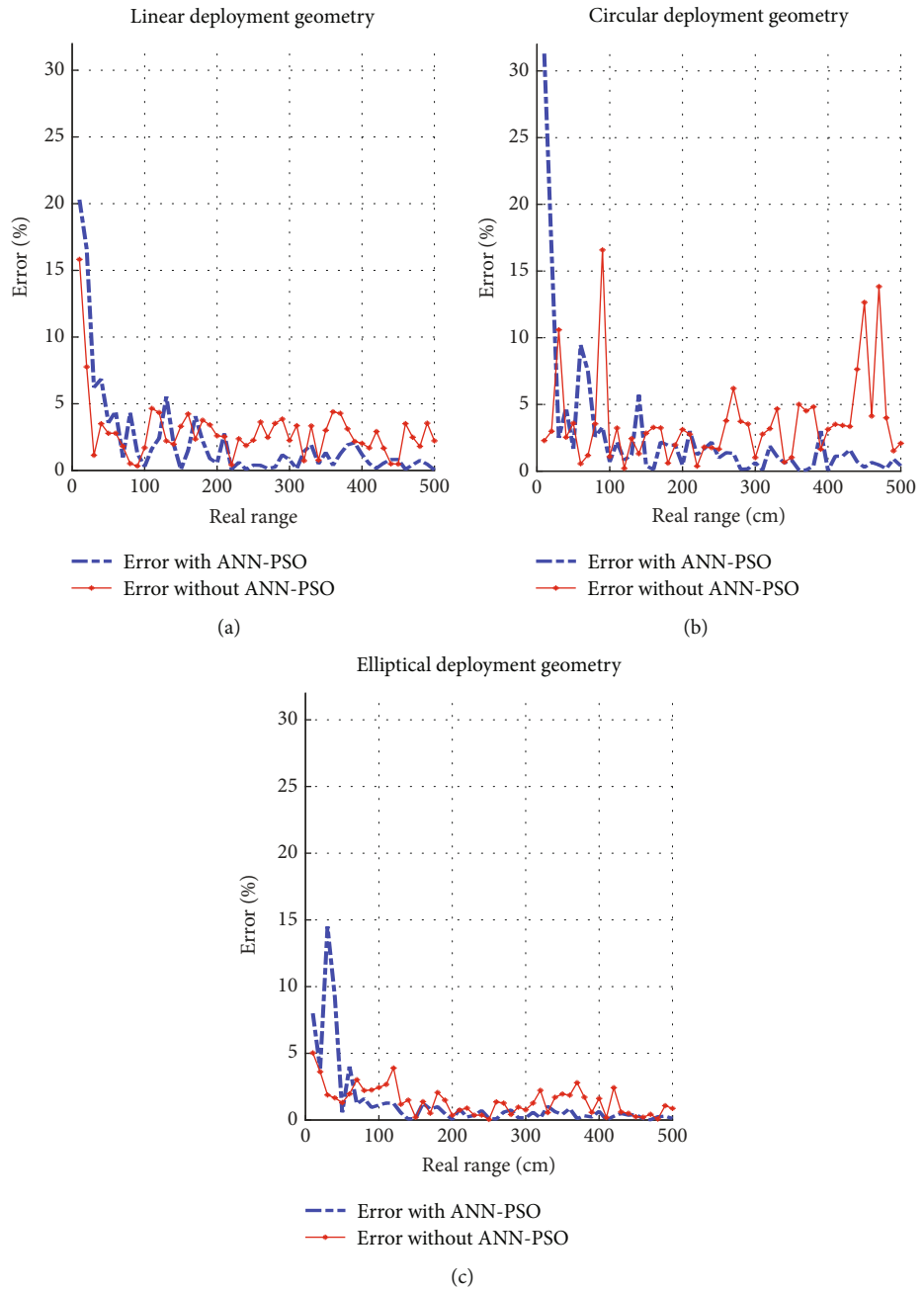


FIGURE 8: Error measurement at regular sensor spacing: (a) linear deployment geometry, (b) circular deployment geometry, and (c) elliptical deployment geometry.

The results in Table 5 show that our method performs better than the results in [79], and that in the mapping domain, it can be used by deploying a multisensor system in elliptical geometry. The elliptical geometry with regular sensor spacing has errors of less than 1%, i.e., an efficiency of more than 99% in the interval [240; 400] cm and less performance in the interval [40; 160] cm.

Figure 8 shows the percentage errors of measurement and prediction, respectively, of the data acquisition device and the proposed data fusion method when deployed under three different regularly spaced geometries. Figure 8(a) shows the measurement errors in the linear deployment geometry. By applying the proposed method, the behavior of the measurements is in three intervals. In the interval [0; 60] cm, we have a maximum error of 20.3% and a minimum of 3.58% more than the actual value, i.e., an average accuracy of 90.338%. Then, in the interval [70; 180] cm, we have a maximum error of 5.538% and a minimum of 0.066% more than the real value, i.e., an average precision of 97.808%. Finally, in the interval [190; 500] cm, the maximum error is 2.762% and the minimum error is 0.04% more than the actual value, i.e., an average accuracy of 99.22%. The analysis in Figure 8(a) shows that using the proposed data fusion method has an overall detection accuracy of

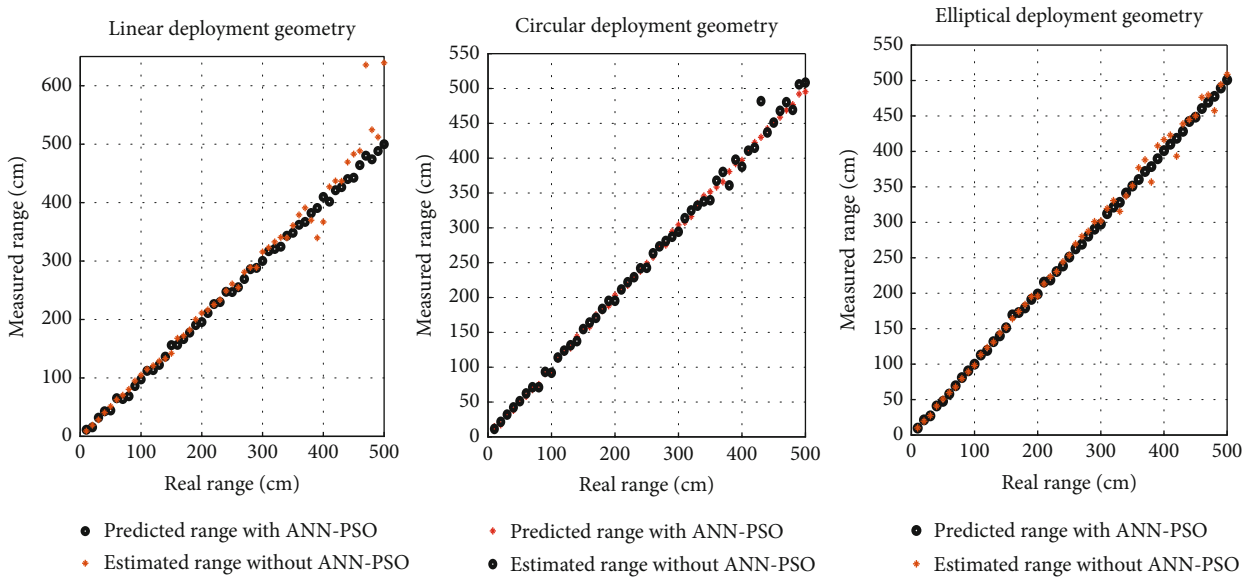


Figure 9: Target-to-device distance estimation under three deployment geometries at irregular spacing.

97.816% and an increase in accuracy of 11.816% in comparison with the results presented in [54, 69] which used a support vector machine classifier.

Figure 8(b) shows the measurement errors in the circular deployment geometry. We notice that by applying the proposed method, the measurement behavior of the span can be divided into three intervals. In the interval [0, 60] cm, the maximum error is 31.3% and the minimum error is 1.68% more than the actual value, i.e., an average accuracy of 88.957%. Then, in the interval [70; 180] cm, the maximum error is 5.714% and the minimum error is 0.125% more than the real value, i.e., an average precision of 97.611%. Finally, in the interval [190; 500] cm, the maximum error is 3% and the minimum error is 0.05% more than the actual value, i.e., an average accuracy of 99.041%. The analysis in Figure 8(b) shows that the proposed method achieves an overall detection accuracy of 96.93%, which is an increase in accuracy of 1.93% less than the results in [80], who used the Monte Carlo method.

Figure 8(c) shows the measurement errors in the elliptical deployment geometry. Note that by applying the proposed method, the measurement behavior of the span can be divided into three intervals. In the interval [0, 60] cm, we have a maximum error of 14.5% and a minimum of 0.58% more than the actual value, i.e., an average accuracy of 93.3075%. Then, in the interval [70; 180] cm, the maximum error is 1.6% and the minimum error is 0.07% more than the real value, i.e., an average precision of 99.067%. Finally, in the interval [190; 500] cm, the maximum error is 1.03% and the minimum is 0% more than the true value, i.e., an average accuracy of 99.632%. The analysis in Figure 8(c) shows that the proposed method achieves an overall detection accuracy of 98.737%, which is 12.737% and 3.737% more accurate than the results in [25, 54, 80], respectively.

Figure 9 shows the target-device range data with irregular spacing between the sensors under three deployment geometries on actual values. The data predicted by the proposed data fusion method (ANN-PSO) are in black, and the raw data are in brown. A comparison of results is made between those predicted by the proposed PSO-ANN fusion method and those estimated by the data acquisition device. A significant improvement in the performance of the multisensor system could be achieved with the algorithm by applying the proposed data fusion method.

In linear, circular, and elliptical geometry along the maximum test range, the measurements follow a quasilinear form in the interval [0; 350] cm. This evolution shows that the signal-to-noise ratio is almost linear over the interval [0; 350] cm. In the interval [360; 500] cm, in linear geometry, the maximum value variation is 10.3 cm with the proposed method and 165.51 cm on the raw data. In circular geometry in the interval [360; 500] cm, the maximum value variation is 9.1 cm by applying the proposed method and the maximum value is 51.88 cm with the raw data. In elliptical geometry in the interval [360; 500] cm, the maximum value variation is 9.5 cm with the proposed method and the maximum value variation is 26.68 cm with the raw data.

An accuracy of 96.81%, 97.089%, and 98.77% have been obtained, respectively, for linear, circular, and elliptical geometries by applying the proposed method. Note that the elliptical geometry has better range estimation accuracy than the circular and linear geometry when the spacing between sensors is irregular.

Figure 10 shows the percentage of errors of measurement and prediction, respectively, of the data acquisition device and the proposed data fusion method under three geometrical deployments in irregular spacing.

Figure 10(a) shows the measurement errors in the linear deployment geometry. Note that by applying the proposed method, the measurement behavior of the range can be divided into three intervals. In the interval [0; 60] cm, the maximum error is 22.558% and the minimum error is 6.467% more than the actual value, i.e., an average accuracy

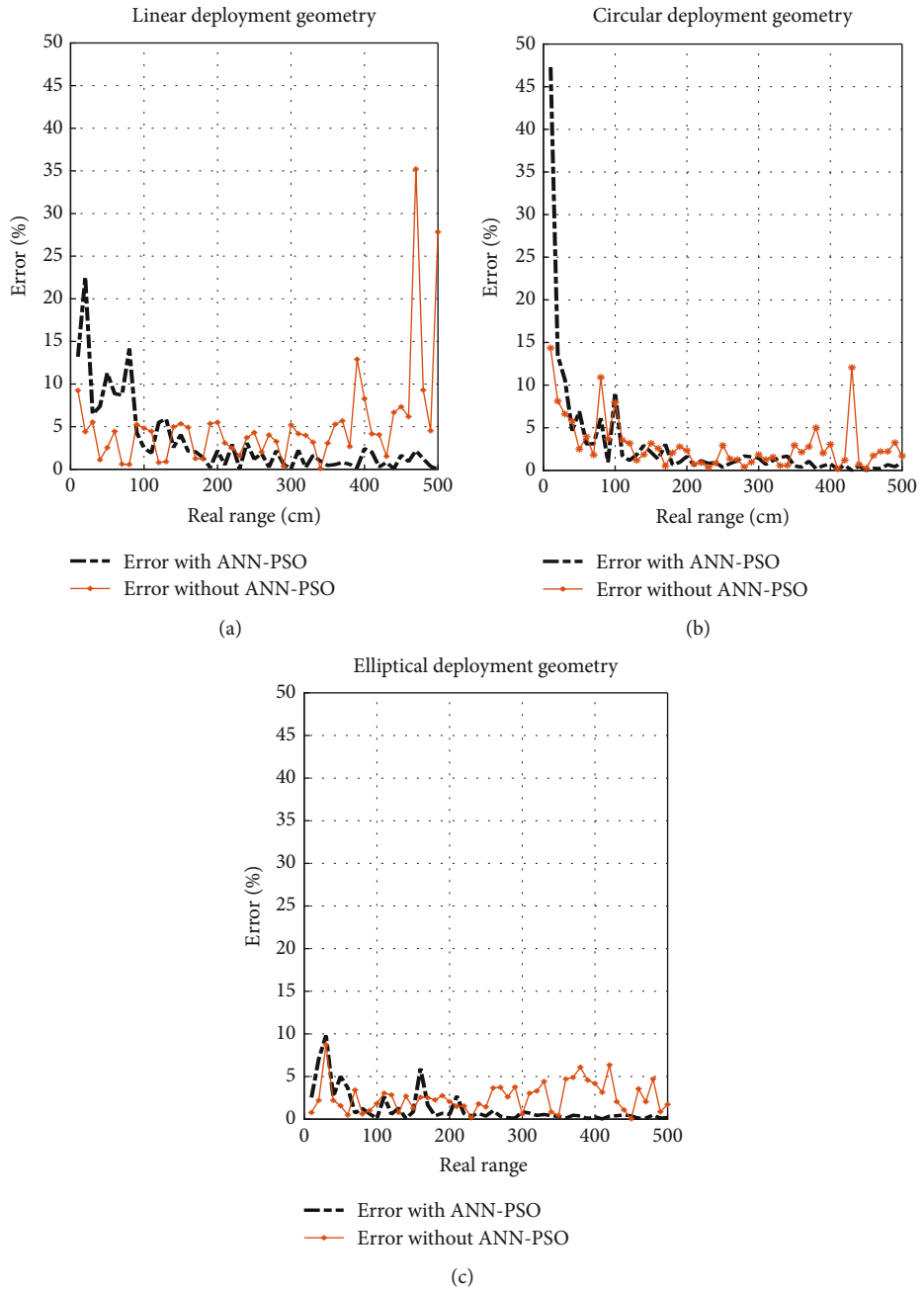


Figure 10: Error measurement at irregular sensor spacing: (a) linear deployment geometry, (b) circular deployment geometry, and (c) elliptical deployment geometry.

of 88.373%. Then, in the interval [70; 180] cm, the maximum error is 14.15% and the minimum error is 1.389% more than the real value, i.e., an average precision of 95.401%. Finally, in the interval [190; 500] cm, the maximum error is 3.083% and the minimum error is 0.02% more than the true value, i.e., an average precision of 98.93%. The analysis of the results presented in Figure 10(a) shows that using the proposed method has an overall detection accuracy of 96.805%, which is an increase in accuracy of 10.805% more than the results in [25, 54] which used a support vector machine classifier.

Figure 10(b) shows the measurement errors in the circular deployment geometry. Note that by applying the proposed method, the behavior of the range measurement can be divided into three intervals. In the interval [0; 60], the maximum error is 47.3% and the minimum error is 3.1% more than the actual value, i.e., an average accuracy of 85.67%. Then, in the interval [70; 180] cm, the maximum error is 9.1% and the minimum error is 0.667% more than the real value, i.e., an average precision of 97.156%. Finally, in the interval [190; 500] cm, the maximum error is 1.676% and the minimum error is 0% more than the true

Table 6: Comparison of the accuracy (%) obtained by the proposed method with that found in the literature.

	Literature							Proposed method					
	Other							Linear		Circular		Elliptical	
Deployment geometry	[81]	[82]	[52]	[66]	[69]	[70]	[72]	RS	IS	RS	IS	RS	IS
Accuracy (%)	86.000	95.000	96.040	45.370	90.300	98.000	97.950	97.810	96.800	96.930	97.080	98.730	98.760

RS: regular spacing; IS: irregular spacing.

Table 7: Calculation results of the errors between the range values predicted by the proposed method and the actual values as a function of spacing.

Error indices	Formula	Deployment geometries					
		Linear		Circular		Elliptical	
		RS	IS	RS	IS	RS	IS
MAPE	$= \frac{1}{n}\sum_{i=1}^{n}\left\|\frac{y_{m(i)} - y_{p(i)}}{y_{m(i)}}\right\|$	$4.37E-04$	$6.38E-04$	$5.02E-04$	$5.82E-04$	$2.52E-04$	$2.46E-04$
MSE	$= \frac{1}{n}\sum_{i=1}^{n}\left\|y_{m(i)} - y_{p(i)}\right\|^2$	0.224	0.464	0.271	0.204	0.051	0.092
MAE	$= \frac{1}{N}\sum_{i=1}^{n}\left\|y_{m(i)} - y_{p(i)}\right\|$	0.052	0.078	0.057	0.054	0.025	0.030

IS: irregular spacing; RS: regular spacing.

value, i.e., an average precision of 99.206%. The analysis of the results presented in Figure 10(b) shows that the proposed method has an overall detection accuracy of 97.088%, which is an increase in accuracy of 2.088% less than the results in [82], who used the Monte Carlo method.

Figure 10(c) shows the measurement errors in the elliptical deployment geometry. Note that by applying the proposed method, the measurement behavior of the span can be divided into three intervals. In the interval [0; 60] cm, the maximum error is 9.8% and the minimum error is 2.625% more than the actual value, i.e., an average accuracy of 94.883%. Then, in the interval [70; 180] cm, the maximum error is 5.938% and the minimum error is 0.09% more than the real value, i.e., an average precision of 98.657%. Finally, in the interval [190; 500] cm, the maximum error is 2.714% and the minimum error is 0.024% more than the true value, i.e., an average precision of 99.536%. The analysis in Figure 8(c) shows that the proposed method has an overall detection accuracy of 98.766%, which is 12.766% and 3.766% more accurate than the results in [54, 80], respectively.

A general remark on the proposed fusion method is that in order to perform well over the interval [0; 60] cm, there is a minimum guard distance to be respected for all sensors to see the target at the same time. This means that the common detection distance for all sensors is the difference between the maximum sensor range and the minimum guard distance.

Table 6 presents a comparison of the estimation accuracies made by the proposed method and those in the literature. It is noted that with the proposed fusion method, whether in linear or circular deployment, a significant improvement in performance is obtained compared to the literature. Note that the elliptical deployment geometry has better results in both regular and nonregular spacing than the linear and circular deployment geometries. The results obtained show that the proposed data fusion method with an accuracy of 10% higher than the results in [54] is a good candidate for the traffic management sector.

In the field of mapping and localization, with more than 2.81% accuracy compared to the results in [79, 80], the proposed method gives significant performance. The health domain is a domain where accuracy is a crucial factor. The proposed method using an elliptical deployment with an accuracy of 0.76% more than the results in [68, 91] can provide better knowledge of the condition of elderly people, and with 0.81% more than the results in [72], it improves the movement of blind people. The proposed method has an average accuracy of 1.2% higher than the results in [9, 92] that are required to save a life in an automobile.

The proposed method can provide a better optimization of building maintenance with 51.71% more than the results in [65]. The field of robotics is booming. Looking at the performance of the proposed method, which has an error of 13 cm less than the results in [57], the proposed method brings more performance. Table 6 shows that the choice and design of the deployment geometry as well as the fusion algorithm are very important parameters for an efficient multisensor data fusion system.

Table 7 shows the expressions for the error indices: mean absolute percentage error (MAPE), mean square error (MSE), and mean absolute error (MAE), where N is the total number of $y_{m(i)}$, the actual data (estimated by the device) used to make the tests, and $y_{p(i)}$ are data predicted by the proposed method. Table 7 shows the results of the calculations of the error indices between the real values and the estimated values (measured by the device) as a function of the deployment geometries committed by the proposed data fusion method. The analysis of the results presented in Table 7 shows us that the mode of spacing between sensors

and the geometry of deployment are crucial parameters in the design of multisensor data collection devices. The spacing and deployment geometry contribute to improving the data fusion. Applying the proposed method, regardless of the geometry, the MAPE is superior to those in [56, 93] which use fuzzy logic. For the MSE, the proposed method provides a better MSE than [25, 61] which uses the Newton polynomial. From Table 7, note that the results for elliptical geometry are better than those for linear and circular geometry, showing the importance of choosing the right deployment geometry for a specific application.

6. Conclusion

This paper proposes a data fusion method to improve the performance of multisensor data acquisition systems. The proposed method includes the design of the data acquisition device, data preprocessing, and data fusion. The false alarm probability and the aperture angle were used to design the deployment geometry of the data acquisition device. Then, for data preprocessing, a synergy algorithm based on the adjustment and compensation factors was proposed to decrease the false alarm detection rate. Finally, for data fusion, the backpropagation neural network with a learning rate and the number of hidden layers optimized by the PSO was used. An identical multisensor prototype was made with the ultrasonic sensors to validate the veracity and practicality of the proposed method on three deployment geometries (linear, circular, and elliptical). These deployment geometries are designed with regular and irregular spacing between the sensors. The results obtained show an overall detection accuracy of 97.300%, 97.000%, and 98.740% in linear, circular, and elliptical geometry, respectively. The proposed merger method is evaluated with indices such as MAPE, MSE, and MAE. The analysis of these results shows that elliptical geometry is better for the acquisition of data from multisensor systems. Future works could focus on improving the proposed method over small distances and adapting the elliptical geometry in the deployment of multistatic radar systems such as synthetic aperture radar. Work needs to be done to optimize the parameters of the PSO, namely, acceleration factors, individual factors, and social factors, allowing the PSO to provide the optimal value of the learning rate and the number of hidden layers in order to have an optimal architecture of the neural network for better data fusion.

Data Availability

Data will be made available on request.

Conflicts of Interest

The authors declare that they have no conflicts of interest.

Authors' Contributions

Luc Eyembe Ihonock was responsible for the conceptualization, validation, investigation, methodology, formal analysis, and writing of the original draft. Jean-François Dikoundou Essiben was responsible for the investigation, supervision, validation, and writing of the original draft. Benjamin Salomon Diboma was responsible for the writing of the original draft, reading, and methodology. Yong Sun Joe reread the original draft and all revised versions of the manuscript.

Supplementary Materials

Supplementary 1. The file (all results of significance testing) presents all the results of the statistical significance test of the data used in the manuscript. This is irregular and regular spacing according to three geometries (linear, circular, and elliptical).

Supplementary 2. The file entitled "Experimental evaluation of the performances of multi-sensors ultrasonic deployment geometries" (https://assets.researchsquare.com/files/rs-2058124/v1_covered.pdf?c=1663711436) is a preprint article that details the design of the elliptical architecture as well as a new formulation for determining the spacing between sensors in a multisensor system. The data collected in this previous work allowed us to validate the data fusion approach proposed in this manuscript.

References

[1] J. Hu, B. Zheng, C. Wang et al., "A survey on multi-sensor fusion based obstacle detection for intelligent ground vehicles in off-road environments," *Frontiers of Information Technology & Electronic Engineering*, vol. 21, no. 5, pp. 675–692, 2020.

[2] R. Adla, Y. Bazzi, and N. Al-holou, "Multi sensor data fusion, methods and problems," *International conference on parallel and distributed processing techniques and applications*, pp. 105–110, 2013, http://world-comp.org/p2013/PDP4248.pdf.

[3] H. S. Carvalho, W. B. Heinzelman, A. L. Murphy, and C. J. N. Coelho, "A general data fusion architecture," *Proceedings of the 6th International Conference on Information Fusion, FUSION 2003*, vol. 2, pp. 1465–1472, 2003.

[4] W. Wang, Q. Zhang, W. Tan, W. Shi, and F. Pang, "Direction finding via acoustic vector sensor array with non-orthogonal factors," *Digital Signal Processing*, vol. 108, article 102910, 2021.

[5] H. Lee, J. Choi, S. Heo, and K. Huh, "Centralized multi-sensor Poisson multi-Bernoulli mixture tracker for autonomous driving," *IFAC-PapersOnLine*, vol. 55, no. 14, pp. 40–45, 2022.

[6] X. Gao, J. Chen, D. Tao, and X. Li, "Multi-sensor centralized fusion without measurement noise covariance by variational Bayesian approximation," *IEEE Transactions on Aerospace and Electronic Systems*, vol. 47, no. 1, pp. 718–727, 2011.

[7] Y. Xiong, B. Liang, H. Yu, J. Chen, Y. Jin, and M. Xing, "Processing of bistatic SAR data with nonlinear trajectory using a controlled-SVD algorithm," *IEEE Journal of Selected Topics in Applied Earth Observations and Remote Sensing*, vol. 14, pp. 5750–5759, 2021.

[8] K.-C. C. Mori, W. H. Barker, Chee-Yee Chong, and Kuo-Chu Chang, "Track association and track fusion with nondeterministic target dynamics," *IEEE Transactions on Aerospace and Electronic Systems*, vol. 38, no. 2, pp. 659–668, 2002.

[9] X. Zhang, T. Wang, W. Luo, and P. Huang, "Multi-level fusion and attention-guided CNN for image dehazing," *IEEE*

Transactions on Circuits and Systems for Video Technology, vol. 31, no. 11, pp. 4162–4173, 2021.

[10] T. Li, Y. Xin, Z. Liu, and K. Da, "Best fit of mixture for multi-sensor Poisson multi-Bernoulli mixture filtering," *Signal Processing*, vol. 202, article 108739, 2023.

[11] W. Jiang, Z. Wei, B. Li, Z. Feng, and Z. Fang, "Improve radar sensing performance of multiple roadside units cooperation via space registration," *IEEE Transactions on Vehicular Technology*, vol. 71, no. 10, pp. 10975–10990, 2022.

[12] W. Ding, X. Jing, Z. Yan, and L. T. Yang, "A survey on data fusion in internet of things: towards secure and privacy-preserving fusion," *Information Fusion*, vol. 51, pp. 129–144, 2019.

[13] Z. Huang, J. Shao, W. Guo, W. Li, J. Zhu, and D. Fang, "Hybrid machine learning-enabled multi-information fusion for indirect measurement of tool flank wear in milling," *Measurement*, vol. 206, article 112255, 2023.

[14] M. Salimibeni and A. Mohammadi, "Hybrid indoor localization via reinforcement learning-based information fusion," 2022, http://arxiv.org/abs/2210.15132.

[15] Y. Lei, H. Qiu, Z. Wang, S. Luo, and Z. Zheng, "Data fusion based multi-rate Kalman filtering with unknown input for on-line estimation of dynamic displacements," *Journal of the International Measurement Confederation*, vol. 131, pp. 211–218, 2019.

[16] V. H. Jaramillo, J. R. Ottewill, R. Dudek, D. Lepiarczyk, and P. Pawlik, "Condition monitoring of distributed systems using two-stage Bayesian inference data fusion," *Mechanical Systems and Signal Processing*, vol. 87, pp. 91–110, 2017.

[17] R. Adhikari and R. K. Agrawal, "Hybridization of artificial neural network and particle swarm optimization methods for time series forecasting," *International Journal of Applied Evolutionary Computation (IJAEC)*, vol. 4, no. 3, pp. 75–90, 2013.

[18] E. Blasch, A. Steinberg, S. Das et al., "Revisiting the JDL model for information exploitation," in *Proceedings of the 16th International Conference on Information Fusion*, pp. 129–136, Istanbul, Turkey, 2013.

[19] R. C. Luo, Y. C. Chou, and O. Chen, "Multisensor fusion and integration: algorithms, applications, and future research directions," in *2007 International Conference on Mechatronics and Automation*, pp. 1986–1991, Harbin, China, 2007.

[20] E. Pollard, B. Pannetier, and M. Rombaut, "Performances in multitarget tracking for convoy detection over real GMTI data," in *2010 13th International Conference on Information Fusion*, Edinburgh, UK, 2010.

[21] J. Bleiholder and F. Naumann, "Data fusion," *ACM Computing Surveys*, vol. 41, no. 1, pp. 1–41, 2009.

[22] J. Yan, H. Jiao, W. Pu, C. Shi, J. Dai, and H. Liu, "Radar sensor network resource allocation for fused target tracking: a brief review," *Information Fusion*, vol. 86, pp. 104–115, 2022.

[23] H. Zheng, A. Cai, Q. Zhou et al., "Optimal preprocessing of serum and urine metabolomic data fusion for staging prostate cancer through design of experiment," *Analytica Chimica Acta*, vol. 991, pp. 68–75, 2017.

[24] J. Duan, X. L. Liu, X. Chen, and Q. Chen, "Unmark AGV tracking method based on particle filtering and LSTM network," *Transducer and Microsystem Technologies*, vol. 39, 2020.

[25] G. I. Gandha and D. Nurcipto, "The performance improvement of the low-cost ultrasonic range finder (HC-SR04) using Newton's polynomial interpolation algorithm," *Informatics-Telecommun. - Electron*, vol. 11, no. 4, pp. 108–113, 2019.

[26] F. Castanedo, "A review of data fusion techniques," *Scientific World Journal*, vol. 2013, article 704504, 19 pages, 2013.

[27] Z. Li, D. Wang, N. Dey, A. S. Ashour, R. S. Sherratt, and F. Shi, "Plantar pressure image fusion for comfort fusion in diabetes mellitus using an improved fuzzy hidden Markov model," *Biocybernetics and Biomedical Engineering*, vol. 39, no. 3, pp. 742–752, 2019.

[28] S. Xiaojun, H. Zhou, H. Shen, and G. Yan, "Weighted fusion robust incremental Kalman filter," *Journal of Electronics and Information Technology*, vol. 43, no. 12, pp. 3580–3686, 2021.

[29] J. B. Xue, H. F. Li, G. Y. Yang, J. Ma, and J. Y. Bi, "A speed estimation method based on adaptive multi-model extended Kalman filter for induction motors," *Micromotors*, vol. 53, 2020.

[30] M. Huang, J. R. Li, L. Z. Gao, S. Qian, and F. C. Wang, "A UKF trajectory tracking algorithm based on multi-sensor robust fusion," *Journal of Air Force Engineering University*, vol. 22, p. 6, 2021.

[31] X. A. Xue and Y. Feng, "Multi-sensor hierarchical weighting fusion algorithm for maneuvering target tracking," *Journal of Detection Control*, vol. 42, no. 5, 2020.

[32] F. Xiao and B. Qin, "A weighted combination method for conflicting evidence in multi-sensor data fusion," *Sensors*, vol. 18, no. 5, 2018.

[33] X. F. Zhao and Z. Wu, "Multi-points parallel information fusion for target recognition of multi- sensors," *Command Control and Simulation*, vol. 42, pp. 23–27, 2020.

[34] J. B. Zheng, R. H. Cen, J. Chen, and Z. H. Xiong, "Fault diagnosis method based on EMD sample entropy and improved DS evidence theory," *Automating Information Engineering*, vol. 41, no. 8, 2020.

[35] E. Brumancia, S. Justin Samuel, L. M. Gladence, and K. Rathan, "Hybrid data fusion model for restricted information using Dempster–Shafer and adaptive neuro-fuzzy inference (DSANFI) system," *Soft Computing*, vol. 23, no. 8, pp. 2637–2644, 2019.

[36] Z. H. Zhu and M. R. Sheng, "Data fusion algorithm of hyubrid multi-sensor based on fuzzy clustering," *Shipboard Electronic Countermeasure*, vol. 42, no. 5, 2019.

[37] T. Meng, X. Jing, Z. Yan, and W. Pedrycz, "A survey on machine learning for data fusion," *Information Fusion*, vol. 57, pp. 115–129, 2020.

[38] C. A. Ke, T. A. Chong, L. I. Hong, and Z. H. H. Min, "Data fusion algorithm of wireless sensor network based on BP neural network optimized by improved grey wolf optimizer," *Journal of University of Chinese Academy of Sciences*, vol. 39, no. 2, pp. 232–239, 2022.

[39] Y. Wang, X. Zhang, M. Lu, H. Wang, and Y. Choe, "Attention augmentation with multi-residual in bidirectional LSTM," *Neurocomputing*, vol. 385, pp. 340–347, 2020.

[40] H. Yin, D. Li, Y. Wang, and X. Hong, "Adaptive data fusion method of multisensors based on LSTM-GWFA hybrid model for tracking dynamic targets," *Sensors*, vol. 22, no. 15, 2022.

[41] C. Fu and S. F. Jiang, "A hybrid data-fusion system by integrating CFD and PNN for structural damage identification," *Applied Sciences*, vol. 11, no. 17, 2021.

[42] J. Cui, P. Xie, X. Wang, J. Wang, Q. He, and G. Jiang, "M2FN: an end-to-end multi-task and multi-sensor fusion network for intelligent fault diagnosis," *Journal of the International Measurement Confederation*, vol. 204, article 112085, 2022.

[43] R. Bai, Q. Xu, Z. Meng, L. Cao, K. Xing, and F. Fan, "Rolling bearing fault diagnosis based on multi-channel convolution neural network and multi-scale clipping fusion data augmentation," *Journal of the International Measurement Confederation*, vol. 184, article 109885, 2021.

[44] T. Han, W. Xie, and Z. Pei, "Semi-supervised adversarial discriminative learning approach for intelligent fault diagnosis of wind turbine," *Information Sciences*, vol. 648, article 119496, 2023.

[45] T. Han and Y. F. Li, "Out-of-distribution detection-assisted trustworthy machinery fault diagnosis approach with uncertainty-aware deep ensembles," *Reliability Engineering & System Safety*, vol. 226, 2022.

[46] Z. He, T. Shi, and J. Xuan, "Milling tool wear prediction using multi-sensor feature fusion based on stacked sparse autoencoders," *Journal of the International Measurement Confederation*, vol. 190, article 110719, 2022.

[47] M. G. Abdolrasol, S. S. Hussain, T. S. Ustun et al., "Artificial neural networks based optimization techniques: a review," *Electronics*, vol. 10, no. 21, p. 2689, 2021.

[48] M. A. Elaziz, A. Dahou, L. Abualigah et al., "Advanced metaheuristic optimization techniques in applications of deep neural networks: a review," *Neural Computing and Applications*, vol. 33, pp. 14079–14099, 2021.

[49] A. Ansari, I. S. Ahmad, and M. R. Yaakub, "A hybrid metaheuristic method in training artificial neural network for bankruptcy prediction," *IEEE Access*, vol. 8, pp. 176640–176650, 2020.

[50] X. Wang, J. Ellul, and G. Azzopardi, "Elderly fall detection systems: a literature survey," *Frontiers in Robotics and AI*, vol. 7, 2020.

[51] I. O. Olayode, L. K. Tartibu, M. O. Okwu, and U. F. Ukaegbu, "Development of a hybrid artificial neural network-particle swarm optimization model for the modelling of traffic flow of vehicles at signalized road intersections," *Applied Sciences*, vol. 11, no. 18, 2021.

[52] J. H. Rhee and J. Seo, "Low-cost curb detection and localization system using multiple ultrasonic sensors," *Sensors*, vol. 19, no. 6, 2019.

[53] C. S. Arvind and J. Senthilnath, "Autonomous vehicle for obstacle detection and avoidance using reinforcement learning," in *Soft Computing for Problem Solving: SocProS*, vol. 1, pp. 55–66, Springer, Singapore, 2018.

[54] G. Li, S. Eben, R. Zou, Y. Liao, and B. Cheng, "Detection of road traffic participants using cost-effective arrayed ultrasonic sensors in low-speed traffic situations," *Mechanical Systems and Signal Processing*, vol. 132, pp. 535–545, 2019.

[55] S. H. Jeong, J. N. Oh, B. S. Kim, M. Kim, and K. H. Lee, "Low cost design of parallel parking assist system based on an ultrasonic sensor," *International Journal of Automotive Technology*, vol. 11, no. 3, pp. 409–416, 2010.

[56] J. Sankar, S. Adarsh, and K. I. Ramachandran, "Performance evaluation of ultrasonic and infrared waves on human body and metal surfaces for mobile robot navigation," *Materials Today Proceedings*, vol. 5, no. 8, pp. 16516–16525, 2018.

[57] T. Wang, C. Tong, and B. Xu, "AGV navigation analysis based on multi-sensor data fusion," *Multimedia Tools and Applications*, vol. 79, no. 7–8, pp. 5109–5124, 2020.

[58] S. E. Li, G. Li, J. Yu et al., "Kalman filter-based tracking of moving objects using linear ultrasonic sensor array for road vehicles," *Mechanical Systems and Signal Processing*, vol. 98, pp. 173–189, 2018.

[59] S. Lee, W. Choi, and D. H. Lee, "Securing ultrasonic sensors against signal injection attacks based on a mathematical model," *IEEE Access*, vol. 7, pp. 107716–107729, 2019.

[60] M. Kelemen, I. Virgala, T. Kelemenová et al., "Distance measurement via using of ultrasonic sensor," *Journal of Automation and Control*, vol. 3, no. 3, pp. 71–74, 2015.

[61] G. I. Gandha and D. A. Santoso, "The Newton's polynomial based - automatic model generation (AMG) for sensor calibration to improve the performance of the low-cost ultrasonic range finder (HC-SR04)," *Jurnal Infotel*, vol. 12, no. 3, pp. 115–122, 2020.

[62] E. N. Budisusila, "Artificial neural network algorithm for autonomous vehicle ultrasonic multi-sensor system," in *2020 10th Electrical Power, Electronics, Communications, Controls and Informatics Seminar (EECCIS)*, pp. 128–131, Malang, Indonesia, 2020.

[63] P. K. Mvemba, S. Kidiamboko, G. Gua, A. Lay-ekuakille, and N. I. Giannoccaro, "Advanced acoustic sensing system on a mobile robot: design, construction and measurements," *IEEE Instrumentation & Measurement Magazine*, vol. 21, no. 2, 2018.

[64] M. Khaoula, Á. Hern, J. M. Villadangos, and M. Machhout, "Evaluation of multi-sensor fusion methods for ultrasonic indoor positioning," *Applied Sciences*, vol. 11, no. 15, p. 6805, 2021.

[65] J. Xiong, L. Shu, Q. Wang, W. Xu, and C. Zhu, "A scheme on indoor tracking of ship dynamic positioning based on distributed multi-sensor data fusion," *IEEE Access*, vol. 5, pp. 379–392, 2017.

[66] N. Moretti, J. D. Blanco Cadena, A. Mannino, T. Poli, and F. Re Cecconi, "Maintenance service optimization in smart buildings through ultrasonic sensors network ultrasonic sensors network," *Intelligent Buildings International*, vol. 13, no. 1, pp. 4–16, 2021.

[67] K. S. Alli, M. O. Onibonoje, A. S. Oluwole et al., "Development of an Arduino-based obstacle avoidance robotic system for an unmanned vehicle," *Journal of Engineering and Applied Science*, vol. 13, no. 3, pp. 886–892, 2018.

[68] S. K. A. Nair, S. Joladarashi, and N. Ganesh, "Evaluation of ultrasonic sensor in robot mapping," in *2019 3rd International Conference on Trends in Electronics and Informatics (ICOEI)*, pp. 638–641, Tirunelveli, India, 2019.

[69] Z. Chen and Y. Wang, "Infrared – ultrasonic sensor fusion for support vector machine – based fall detection," *Journal of Intelligent Material Systems and Structures*, vol. 29, no. 9, pp. 2027–2039, 2018.

[70] C. Nadee and K. Chamnongthai, "An ultrasonic-based sensor system for elderly fall monitoring in a smart room," *Journal of Healthcare Engineering*, vol. 2022, Article ID 2212020, 21 pages, 2022.

[71] N. Amin and M. Borschbach, "Quality of obstacle distance measurement using ultrasonic sensor and precision of two computer vision-based obstacle detection approaches," in *2015 International Conference on Smart Sensors and Systems (IC-SSS)*, Bangalore, India, 2015.

[72] C. Gearhart, A. Herold, B. Self, C. Birdsong, and L. Slivovsky, "Use of ultrasonic sensors in the development of an electronic travel aid," in *2009 IEEE Sensors Applications Symposium*, New Orleans, LA, USA, 2009.

[73] N. S. Ahmad, N. L. Boon, and P. Goh, "Multi-sensor obstacle detection system via model-based state-feedback control in smart cane design for the visually challenged," *IEEE Access*, vol. 6, pp. 64182–64192, 2018.

[74] Y. Rohilla, V. Parihar, and K. K. Rohilla, "Ultrasonic sensor based smart cap as electronic travel aid for blind people," in *2020 Third International Conference on Smart Systems and Inventive Technology (ICSSIT)*, Tirunelveli, India, 2020.

[75] G. Laštovička-Medin, "Social engineering and prototype awareness enhancing during international coronavirus outbreak," in *2020 9th Mediterranean Conference on Embedded Computing (MECO)*, Budva, Montenegro, 2020.

[76] B. M. Nagabhushana and S. Ali, "Ultrasonic detection and signal response of polymers in aquatic environment: using Arduino microcontroller," in *2017 Dynamics of Systems, Mechanisms and Machines (Dynamics)*, Omsk, Russia, 2017.

[77] O. Bereziuk, M. Lemeshev, V. Bogachuk, W. Wójcik, K. Nurseitova, and A. Bugubayeva, "Ultrasonic microcontroller device for distance measuring between dustcart and container of municipal solid wastes," *Przeglad Elektrotechniczny*, no. 4, pp. 146–150, 2019.

[78] G. Montazeaud, C. Langrume, S. Moinard et al., "Development of a low cost open-source ultrasonic device for plant height measurements," *Smart Agricultural Technology*, vol. 1, article 100022, 2021.

[79] H. R. Hatem, A. I. Abdalla, and Z. N. A. Al-rawi, "Design and implementation of ultrasonic radar system for distance measurements using Arduino," *International Journal of Engineering & Technology*, vol. 7, no. 4, 2018.

[80] C. Kundu, P. Patra, B. Tudu, and R. Bandyopadhyay, "Novel method for real-time burden profile measurement at blast furnace," *Ironmaking & Steelmaking*, vol. 48, no. 5, pp. 579–585, 2021.

[81] A. Tedeschi, S. Calcaterra, and F. Benedetto, "Ultrasonic radar system (URAS): Arduino and virtual reality for a light-free mapping of indoor environments," *IEEE Sensors Journal*, vol. 17, no. 14, pp. 4595–4604, 2017.

[82] B. Qin, S. D. Pendleton, V. Technologies, and M. H. A. Jr, "Sensor fusion for localization, mapping and navigation in an indoor environment," in *2014 International Conference on Humanoid, Nanotechnology, Information Technology, Communication and Control, Environment and Management (HNICEM)*, Palawan, Philippines, 2014.

[83] H. Chen, H. Chen, Y. Xu, D. Zhang, Y. Ma, and J. Mao, "Research on attitude monitoring method of advanced hydraulic support based on multi-sensor fusion," *Measurement*, vol. 187, article 110341, 2022.

[84] P. G. Zhang, "Time series forecasting using a hybrid ARIMA and neural network model," *Neurocomputing*, vol. 50, pp. 159–175, 2003.

[85] D. T. Viet, V. Van Phuong, M. Q. Duong, A. Kies, B. U. Schyska, and Y. K. Wu, "A short-term wind power forecasting tool for Vietnamese wind farms and electricity market," in *2018 4th International Conference on Green Technology and Sustainable Development (GTSD)*, pp. 130–135, Ho Chi Minh City, Vietnam, 2020.

[86] T. Trung, N. Thuan, T. Nguyen, and M. Quan, "An improved equilibrium optimizer for optimal placement of photovoltaic systems in radial distribution power networks," *Neural Computing and Applications*, vol. 123456789, no. 34, pp. 6148–6779, 2022.

[87] C. Kihoro, J. M. Otieno, and R. O. Wafula, "Seasonal time series forecasting: a comparative study of ARIMA and ANN models," *African Journal of Science and Technology*, vol. 5, no. 2, pp. 41–50, 2006.

[88] G. K. Jha, P. Thulasiraman, and R. K. Thulasiram, "PSO based neural network for time series forecasting," in *2009 International Joint Conference on Neural Networks*, pp. 1422–1427, Atlanta, GA, USA, 2009.

[89] W. Ali and S. Malebary, "Particle swarm optimization-based feature weighting for improving intelligent phishing website detection," *IEEE Access*, vol. 8, pp. 116766–116780, 2020.

[90] L. I. Eyembe and Y. S. Joe, *Experimental evaluation of the performances of multi-sensors ultrasonic deployment geometries*, Reseach Sq, 2022.

[91] Y. Wei, Z. Cheng, B. Zhu, X. Zhai, and H. Zhang, "Infrared and radar fusion detection method based on heterogeneous data preprocessing," *Optical and Quantum Electronics*, vol. 51, no. 10, 2019.

[92] C.-D. Wann, "Application of self-organizing neural networks to multiradar data fusion," *Optical Engineering*, vol. 36, no. 3, p. 799, 1997.

[93] K. L. Narayanan, R. S. Krishnan, L. H. Son et al., "Fuzzy guided autonomous nursing robot through wireless beacon network," *Multimedia Tools and Applications*, vol. 81, pp. 3297–3325, 2022.